Open-cycle gas turbines: Predicting and controlling far-field noise

Ben Cazzolato (1), Orddom Leav (1) and Carl Howard (1)

(1) School of Electrical and Mechanical Engineering, The University of Adelaide, Australia

Abstract - With exhaust sound power levels often exceeding 150 dB re 1pW, temperatures between 550-650°C, and high flow rates, the mitigation of the noise from large gas turbines used in simple and combined-cycle power stations present a challenge to acoustic engineers, especially under certain atmospheric conditions. This paper presents the research conducted at The University of Adelaide over the last decade on the mechanisms of sound radiation from hot exhausts, how this is affected by local atmospheric conditions as it propagates to the far-field, and potential methods for attenuating this noise. It will be shown that in unfavourable conditions, the sound pressure levels at a nearby community can be 10 dB higher than predicted by commonly used models/standards. However, with the installation of a compact device, this increase in far-field noise can be mostly mitigated. The paper includes results from field measurements near power stations, numerical modelling, small-scale laboratory experiments and recent medium-scale field trials.

1 INTRODUCTION

As the world transitions to renewable sources of electricity, open-cycle gas turbine (OCGT) power plants are being used to provide dispatchable power. These plants are known for generating considerable acoustic energy, and have a history of leading to low frequency community noise (Hessler, 2004; Hetzel & Robert, 2009).

The very high temperatures from the gas turbines (with modern heavy-duty units approaching $T = 700^{\circ}$ C) and high flow speeds (often exceeding Mach $M = 0.1$) present challenges for acoustic engineers when designing the silencers. The high temperatures drive changes in wavelength, viscosity and flow rates: wavelength increases with $\sqrt{T}$, decreases viscosity with $\sqrt{1/T}$, and increases volumetric flow with T. This acts to reduce the efficacy of silencers for a given size, as well as increasing self-noise. To illustrate this, Figure 1 displays one-third octave band sound pressure levels (SPLs) for numerous gas turbines, where the OASPLs at the exhaust outlet for the hotter OCGTs are 20 dB larger compared to the cooler combined-cycle gas turbine (CCGT) plants.

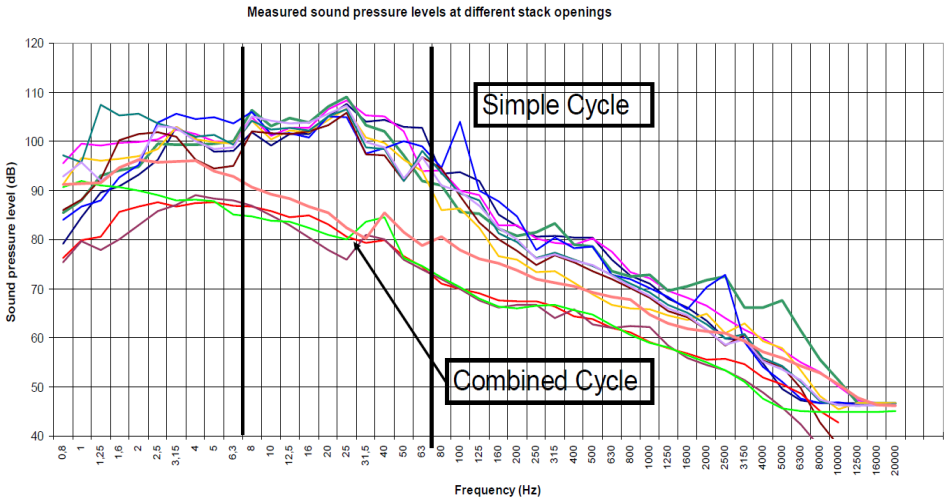

Figure 1 – Sound pressure levels measured on different gas turbine stack openings (Hetzel & Robert, 2009).

Not only are the exhaust SPLs of OCGT plants higher than the CCGT plants, the higher exhaust temperatures and velocities in the plume lead to strong aero-acoustic interactions in the near- and mid-geometric fields, which act to refract the sound away from the plume, ultimately leading to increased SPLs on the ground. This paper explores this phenomenon by documenting a decade of research by The University of Adelaide on how sound propagates from high-temperature exhausts in crosswinds, in particular OCGTs, and potential solutions for decreasing community noise using a novel porous nozzle.

2 MOTIVATION AND BACKGROUND

In 2012, staff from the University of Adelaide studied the noise from a grid-scale OCGT power plant impacting on sensitive receivers. For the most part, far-field predictions matched measurements and met regulatory requirements. However, under certain meteorological conditions (temperature inversions and gentle crosswinds) SPLs downwind and some distance from the source exceeded predicted levels. The noise from the plant contained considerable low-frequency energy and was found to vary considerably over the period of hours, despite no significant change in plant or meteorological conditions. This is illustrated in Figure 2, which shows the normalised OASPLs at a location over 1 km from the plant over a period of 7 hours one evening.

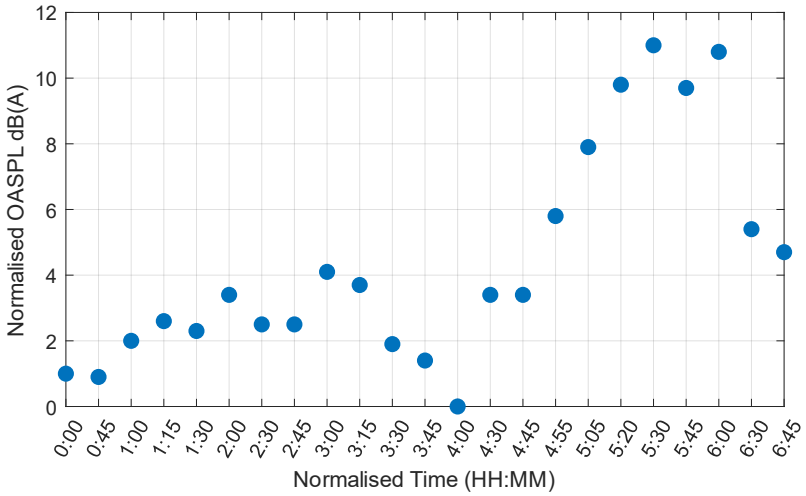

Figure 2 – Sound pressure levels over a 7-hour period at a location >1km from outlet.

Whilst environmental propagation models/standards attempt to quantify uncertainty, they do not predict the variability observed in Figure 2, especially under stable conditions. For example, (ISO 9613-2) estimates accuracy "… at a given site on a given day … can be expected to be considerably larger than … ±3 dB", and CONCAWE (Manning, 1981) suggests 95% confidence limits of approximately ±5 dB(A), with individual octave bands ~±10 dB. This raises the question; how can downwind SPLs vary by over 10 dB despite stable plant and environmental conditions? The answer lies in the sound directivity of the exhaust.

Most environmental noise models of sound radiation from an exhaust stack will use monopole radiation (as shown in Figure 3(a), or use a frequency-dependent model with increasing directivity above $ka = 1$, where $k = \frac{\omega}{c}$ is the wavenumber, ω is the circular frequency, c is the speed of sound, and $a = 0.5D$ is the stack radius. However, it has been known since the mid-60's that sound in heated jets refracts from the plume, and at the far-field limit, almost no acoustic energy remains within the jet as illustrated in Figure 3(b). This is demonstrated in Figure 4, where (a) shows the SPL directivity around a jet for Mach numbers $0 \leq M \leq 0.9$, (b) SPL directivity versus temperature $100°\mathrm{F} \leq T \leq 500°\mathrm{F}$ $(38°\mathrm{C} \leq T \leq 260°\mathrm{C})$, and (c) the attenuation of SPL on-axis as a function of distance from the jet outlet.

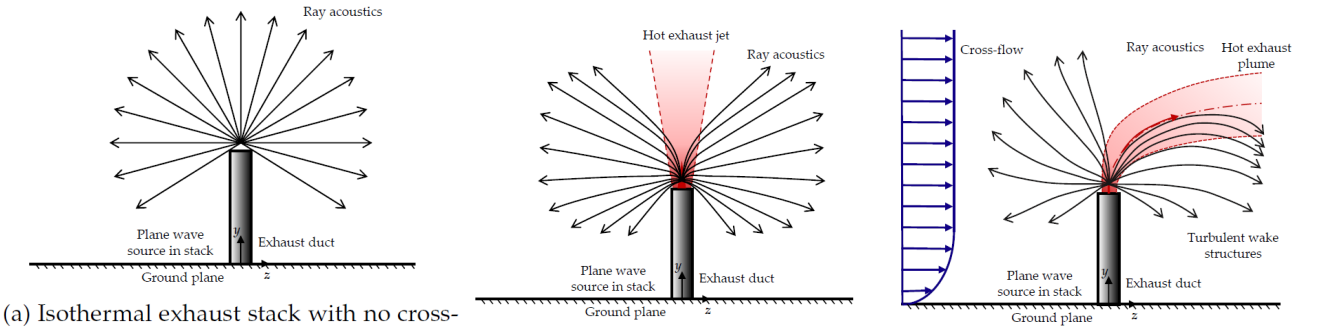

(a) Isothermal exhaust stack with no cross-flow sound propagation (b) Sound propagation with a heated jet (c) Sound propagation with a heated JICF

Figure 3 – Schematic of sound radiation from a monopole, columnated vertical jet, and jet in crossflow (Leav O. , 2020).

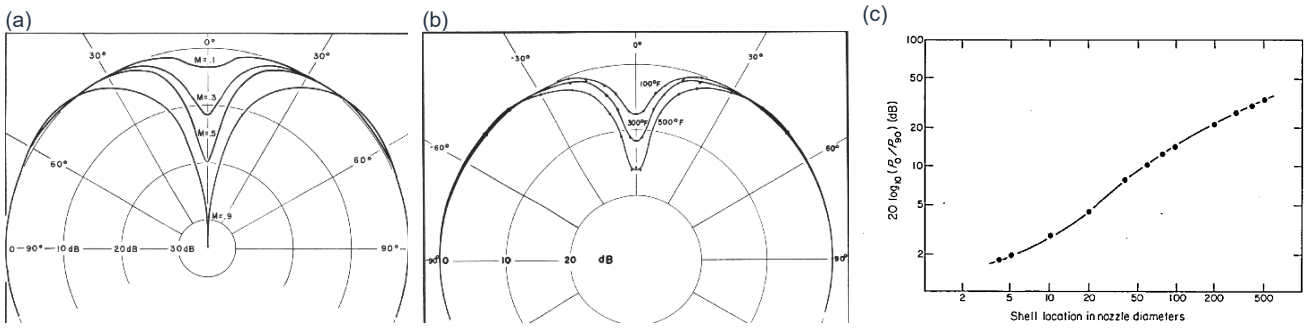

Figure 4 – Sound radiation from a jet a) directivity versus Mach number M (Atvars, Schubert, & Ribner, 1965), b) directivity versus temperature T (Atvars, Schubert, Grande, & Ribner, 1966), and c) SPL attenuation along jet centreline versus distance (Mungur, Plumblee, & Doak, 1974).

The energy that is refracted from the jet plume is conserved, and leads to an increase in SPLs away from the jet. If all the acoustic energy were to refract from the column above the exhaust outlet out to an elevation angle θ (see grey shell in Figure 5(a)), then the average increase in SPL for the remaining part of the hemisphere (orange shell in Figure 5(a)) would be

$$\Delta L_p = -10\,log_{10}(sin\,\theta)\;\; dB. \tag{1}$$

If one assumes $\theta = 45°$ (which represents an extreme case and would only happen for very hot, fast diffuse jets), the increase in average SPL away from the jet would be no more than $\Delta L_p(\theta = 45°) \approx 1.5\text{dB}$, which is insufficient to account for the increased SPLs observed in Figure 2. However, it does demonstrate that acoustic engineers should expect an increase in SPLs due to refraction when dealing with noise from turbomachinery and reciprocating engines. Given acoustic energy is refracted from the plume, the logical extension is to ask what happens to the plume and thus the sound field in the presence of crossflow? Does the sound get refracted down to the ground as illustrated in Figure 3(c), and if so, what SPLs might be expected?

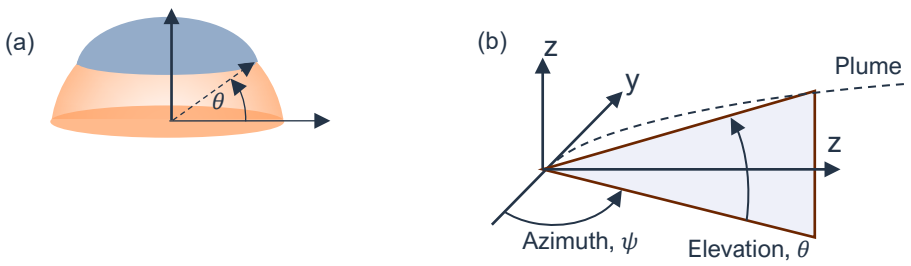

Figure 5 – (a) Section of a hemisphere, b) azimuth and elevation used to define a plume.

For spherical spreading one expects a –6 dB doubling in distance, or –20 dB for a tenfold increase in distance. This reduction in SPL comes from geometric spreading along the azimuth (–3 dB doubling in distance), as well as the elevation (–3 dB doubling in distance) as shown in Figure 5(b). However, when the sound is constrained

vertically, such that the elevation angle $\theta < \pi/2$, then the geometric expansion rate downwind will fall, leading to a relative increase in SPL.

The trajectory for the plume centreline (see Figure 5(b)) can be used to estimate the increase in SPL downstream of the exhaust outlet. For a non-buoyant (cold) plume, the centreline can be approximated by (Bradbury, 1981)

$$\frac{Z}{D} = 0.975 \left(\frac{X}{D}\right)^{0.333} \alpha^{0.9}, \quad (2)$$

where Z is the height above the jet outlet, X is horizontal distance downwind, D is the exhaust diameter, and $\alpha = \frac{v_{\text{jet}}}{v_{\text{crossflow}}}$ is the jet velocity ratio. In the far-field we can use small angle assumption, i.e. elevation $\theta \ll 1$, where it can be shown that the increase in SPL downwind (compared to spherical spreading) can be estimated by

$$\Delta L_p \left(\frac{X}{D}\right) = 6.7\, log_{10} \left(\frac{X}{D}\right) - 9\, log_{10}\, \alpha + 2 \quad dB. \quad (3)$$

As an example, for a crossflow velocity ratio of $\alpha = 4$ and 200 diameters downstream (the location of the receiver in Figure 2), the expected increase is 11 dB. This is remarkably similar to the values observed in Figure 2. In deriving Equation (3), numerous assumptions were made, namely that half of all energy in the plane of the crosswind is concentrated below the plume, and that sound is not refracted out of this plane by the plume. This presents a worst case, since whilst the counter-rotating vortex pairs (a dominant feature of jets in crossflow) are inward refracting, the effect of temperature is outward refracting and is likely to dominate.

Despite the assumptions made when deriving Equation (3), it suggests that perhaps the increase in SPLs downwind from OCGTs could be associated with sound refraction by the plume. The remainder of the paper comprises two parts: Section 3 provides evidence of refraction in crossflows, and Section 4 looks at ways this issue might be mitigated. Section 3 starts with a small 1:200 experimental model without crossflow tested in the Anechoic Chamber at The University of Adelaide, a larger 1:125 experimental model in The University of Adelaide Wind Tunnel in the presence of crossflow, then field trials of a 1:60 scale model using a laboratory gas turbine, and finally numerical models using a coupled CFD-FEA aero-acoustic model solved on a supercomputer. In Section 4, both numerical simulations and scale experiments demonstrate that it is possible to partially mitigate the downwind refraction of sound from hot exhausts using porous nozzles. The following content draws heavily from work previously published by the authors and is referenced appropriately.

3 MODELLING OF SOUND PROPAGATION IN JETS IN CROSSFLOW

3.1 Anechoic chamber experiments 1:200 scale

To explore the how sound is refracted by hot jets (Cazzolato, Hansen, Robertson, & Zhao, 2013) built a small (27 mm internal diameter) 1:200 scale-model of a gas turbine power station exhaust and is shown in Figure 6. The system was supplied with compressed air that was throttled using a regulator, and heated using four heating coils controlled using a Variac. Sound was driven into the base of the exhaust using a compression driver, which provided a coherent noise source to measure the sound directivity. The sound was measured using a circular microphone array at a radius of 1000 mm (37 duct diameters). The flow rate was measured with pitot tubes, and the temperature with thermocouples. The cut-on frequency for the duct at ambient (20°C) was approximately 7.5 kHz. At approximately $f \approx 4$ kHz, the Helmholtz number was unity ($ka = 1$), at which the radiation pattern in the absence of the jet is elliptical.

The test results are shown in Figure 7 demonstrating refraction of sound from the vertical axis as a function of flow rate and temperature, for a temperature-dependent Helmholtz number of $ka \approx 0.8 - 1.2$. These results largely replicated previously published findings (e.g. Figure 4) and were used to validate Equation (1).

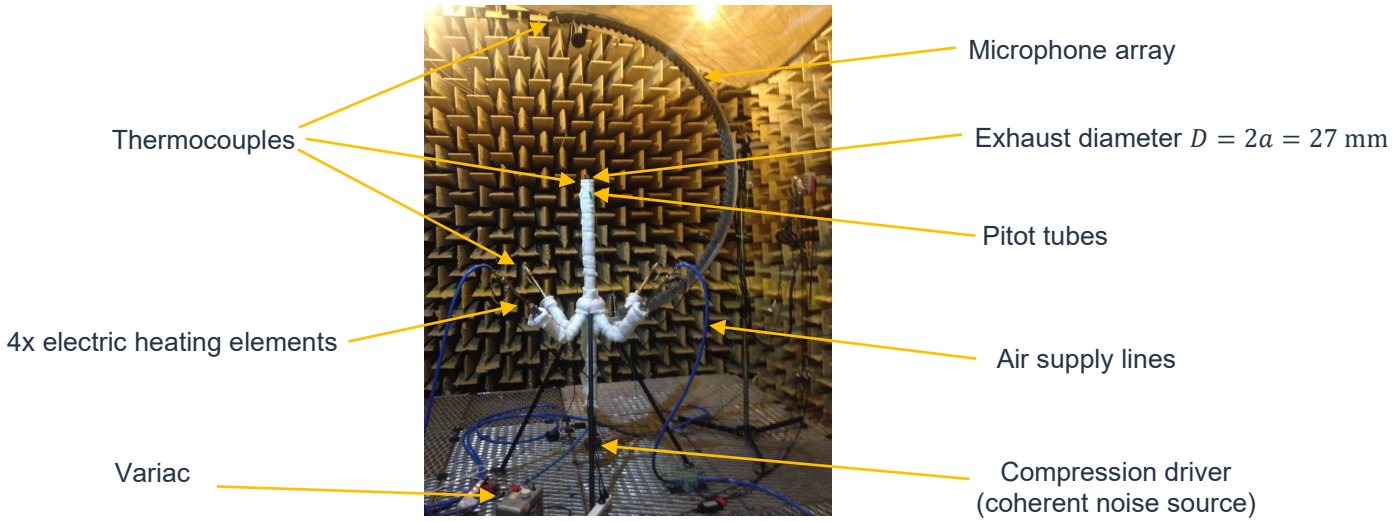

Figure 6 – 1:200 scale model of an OCGT in the Anechoic Chamber at The University of Adelaide.

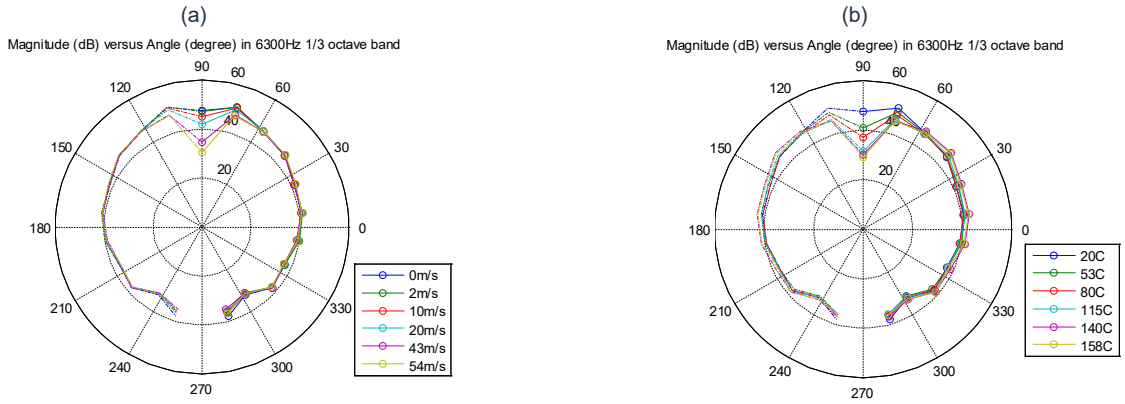

Figure 7 – Sound directivity from a vertical jet, (a) versus jet velocity (ambient jet temperature), and (b) versus temperature (jet velocity ~50 m/s). SPLs were normalised against $\theta = 0°$. From (Cazzolato, Hansen, Robertson, & Zhao, 2013).

3.2 Wind tunnel experiments 1:125 scale

Subsequent to the tests detailed in Section 3.1, a larger 1:125 scale (47.6 mm diameter) stack was built and installed in the University of Adelaide Wind Tunnel, details of which can be found in (Leav O. , 2020) and (Leav, Cazzolato, & Howard, 2021). The hot jet was generated using a Leister Airpack blower and two 16kW Leister LHS 61L regulated heaters, along with an inlet and outlet silencer, compression drivers as a coherent noise source, and a flow straightener (catalytic converter) as shown in Figure 8. The directivity from the exhaust stack was measured using GRAS 40PH ¼" array microphones installed on two semi-circular arrays at a radius of $14D$ and $28D$ from the exhaust (Figure 9(b)). Reflections from the ground plane were minimised with 50 mm thick polyester batts, and reflections from walls and ceilings were suppressed using temporal gating. The wind tunnel was operated as an open tunnel with working section of 3.5 m x 5.5 m to create a crossflow of up to 15 m/s (Figure 9(a)).

The results from the wind tunnel experiments are summarised in Figure 10 for no flow, a vertical hot jet with no crossflow, and a vertical hot jet with crossflow for a Helmholtz number of $ka = 0.85$. For the homogenous media the pattern is elliptical and matches the expected directivity from an open pipe below cut-on. Figure 10(b) shows sound being refracted from the centreline of the hot vertical exhaust, with lobes peaking between $40 - 50°$ from the vertical depending on the wavenumber, quantitatively and qualitatively reflecting the work of others (Section 2). In the presence of crossflow, there is little change to directivity upwind. However, downwind the lobes are pushed towards the ground plane. The impact of distance from the outlet is evident, with directivity yet to converge at $28D$. The SPLs on the ground plane were found to increase between 5–7 dB from a monopole assumption depending on wavenumber, and 10–12 dB increase over the homogenous media (no jet) case.

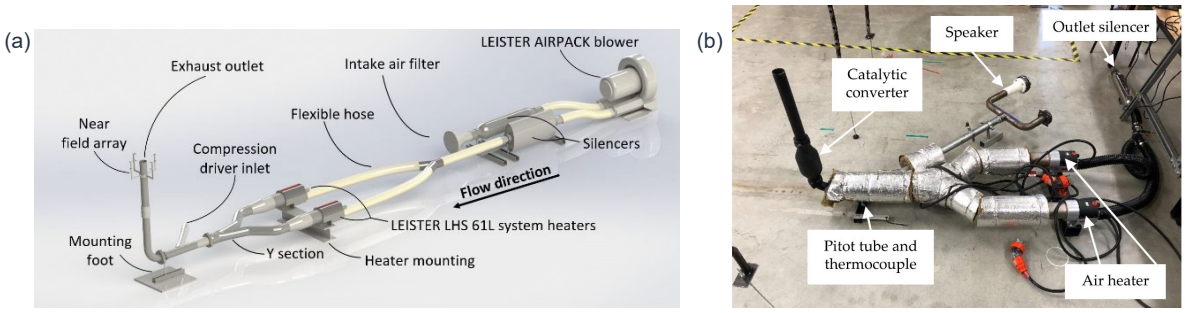

Figure 8 – 1:125 experimental model comprising blower, silencers, heaters, compression driver, flow straightener (catalytic converter) and near-field microphone array (a) solid model, (b) physical model.

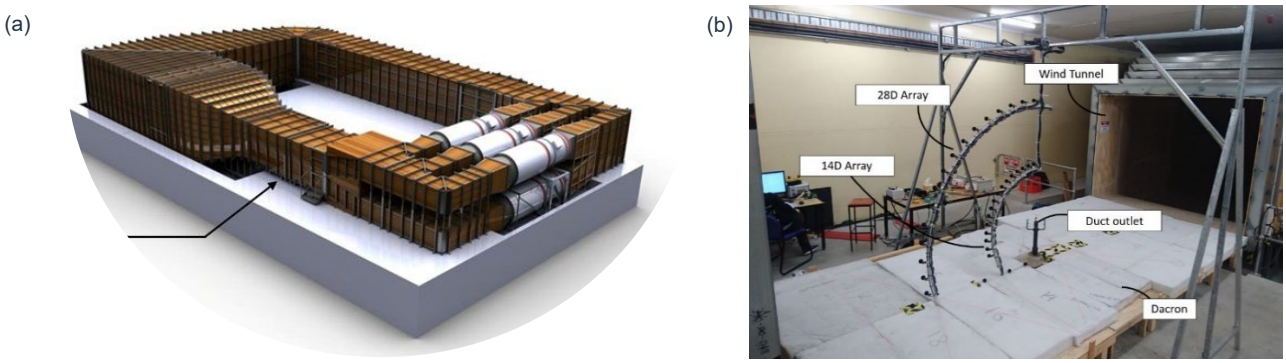

Figure 9 – Adelaide Wind Tunnel. (a) model of the tunnel in the closed configuration, (b) photograph of the open section of the wind tunnel showing exhaust outlet, two microphone arrays at 14D and 28D, and an absorptive ground plane.

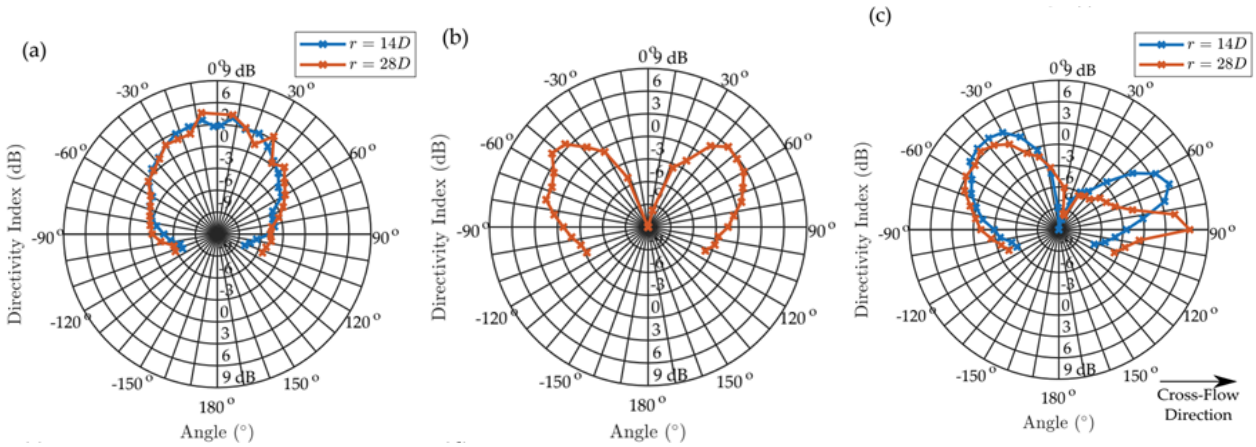

Figure 10 – Results from 1:125 scale experiments for Helmholtz number of $ka = 0.85$. For cases with flow, the exhaust velocity was $M_j = 0.1$, temperature of $T_j = 500°C$, and crossflow momentum ratio $R = 5$. (a) Absence of jet and crossflow, (b) hot jet only, and (c) hot jet with crossflow.

3.3 Field experiments on a 1:60 scale turbojet engine

Whilst the wind tunnel (Section 3.2) provided a stable and controlled environment for investigating the impact of jet velocity and temperature, and crossflow velocity on sound directivity, the sound measurements were limited to a distance of $28D$ from the outlet. Furthermore, the windspeed profile was uniform as opposed to the real-world that has a strong vertical velocity gradient due to the atmospheric boundary layer. Consequently, field trials were undertaken at The University of Adelaide's Buckland Park facility (Figure 11(a)) in 2020/21 using a 250 kW Turbine Technologies SR-30 gas turbine with an exhaust diameter of 100 mm. This represents a doubling in length scale (to 1:60) of the exhaust system compared to the wind tunnel apparatus. Importantly, it permitted far-field measurements of sound at non-dimensional distances ($> 200D$) needed to predict community noise from OCGTs. This work was supported by a AAS Research Grant.

The system comprises a 12 bladed centrifugal flow compressor, combustor and axial flow turbine, with a maximum operating speed of 87,000 RPM, and a maximum exhaust gas temperature of $720°C$. The turbine was installed in a 20-foot insulated shipping container (Figure 11(b) and (c)), then fitted with an inlet suppressor to reduce sound radiation from the intake stage, and the exhaust silencer was removed to increase the sound power transmitted to the exhaust outlet. The turbine was operated at two shaft speeds, approximately 45,000 RPM and 75,000 RPM, delivering exhaust jet flow speeds and temperatures of Mach $M_j = 0.06 - 0.12$ and $T_j = 400° - 560°C$, respectively, and with wind conditions ranging from calm to 8 m/s. The work detailed below has been published previously in (Cazzolato, Leav, & Howard, 2021) and (Cazzolato, Leav, & Howard, 2023).

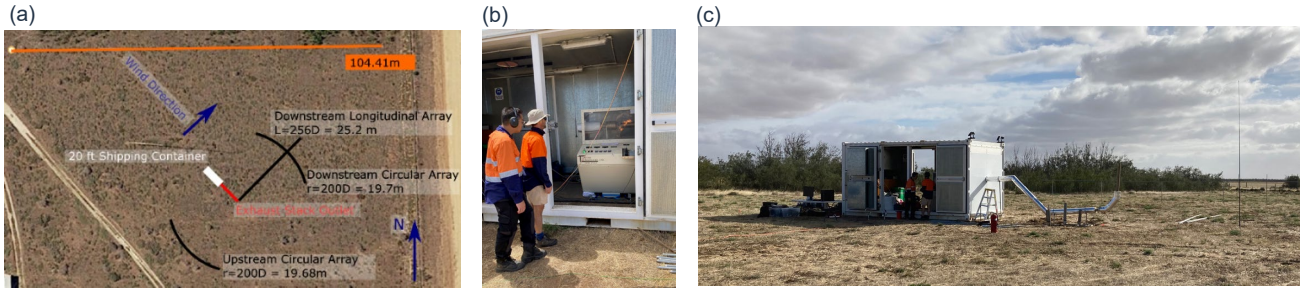

Figure 11 – (a) Geometry of the test site, showing shipping container, exhaust duct, linear and circular microphone arrays, (b) SR-30 turbojet engine on startup, (c) genset shipping container, and exhaust.

Fixed microphone arrays: The noise radiated from the gas turbine was measured in the exhaust plane (2 m height) using two types of fixed microphone arrays: a longitudinal array and two circular arrays shown in Figure 12. The longitudinal array, designed to quantify the geometric spreading rate, consisted of six microphones logarithmically spaced at 8, 16, 32, 64, 128 and 256 exhaust diameters, D, from the exhaust outlet. The two circular arrays spanning $\pm 30°$ were used to quantify the radiation pattern upstream and downstream of the exhaust at a distance of $200D$. GRAS 40PH ¼" free-field IEPE microphones with windscreens were used and recorded at a sample rate of 25.6 kHz for 120 s using a National Instruments PXIe-1073 chassis and NI PXIe-4499 DAQ cards. All microphones were calibrated with a Bruel and Kjaer 4231 with a ¼" adaptor.

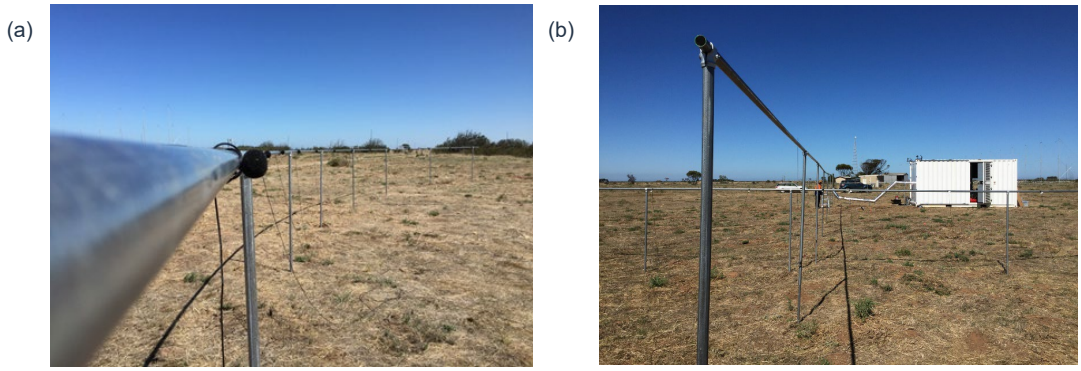

Figure 12 – (a) Upwind circular microphone array, (b) Longitudinal array and downwind circular microphone array.

Acoustic cameras: Three acoustic cameras (Figure 13) were used during the experiments to visualise the radiation patterns. A portable SoundCam comprising 64 microphones, with a 300 mm aperture sampled at 48 kHz with 24-bit precision with a recommended operating range above 800 Hz, and two gfai tech 48 microphone acoustic cameras: a Ring48 AC Pro ring array with an aperture of 750 mm and recommended operating frequency range of 164 Hz–20 kHz, and a Star48 AC Pro star array with an aperture of 3.4 m with recommended operating frequencies from 66 Hz–13 kHz, with data recorded on a gfai tech data recorder 721B.

Roving SLM: A Bruel and Kjaer 2270 Sound Level Meter (SLM) was used to undertake roving measurements at two heights: 1 m and 3 m, i.e., ±1 m from the exhaust outlet plane (and can be seen in the background of Figure 13(a)). The lower microphone was a Bruel and Kjaer 4189 ½" free-field microphone, and the upper microphone was a GRAS 146AE ½" free-field microphone. Both microphones were calibrated using a Bruel and Kjaer 4231 calibrator and then fitted with windshields.

Figure 13 – Acoustic cameras (a) SoundCam (Resonate), (b) gfai tech ring array and star array, (c) gfai tech star array (HW Technologies).

Wind and turbine exhaust measurements: The trials recorded turbine data, exhaust temperatures, exhaust flow rate, wind speed, and wind direction. The turbine data including rotational speed in RPM and exhaust gas temperature were obtained from the control panel of the SR-30. Three k-type thermocouples attached to the exhaust system were used to measure the inlet, gas turbine exhaust and the exhaust outlet temperatures, and were logged simultaneously with the array microphone signals. The wind was measured by a RI-SO P2546A anemometer and an R.M. Young Model 81005A three-axis ultrasonic anemometer, which provided both wind speed and direction. Analog signals from the two anemometers were recorded using a NI-PXI 6221, with a sampling frequency of 25.6 kHz. The exhaust flow speed was measured using a Fluke 922 flow meter and a Testo high temperature Inconel pitot-tube. A streamer mounted on a pole adjacent to the stack outlet identified when the longitudinal array was ‘upstream’ or ‘downstream’ of the outlet.

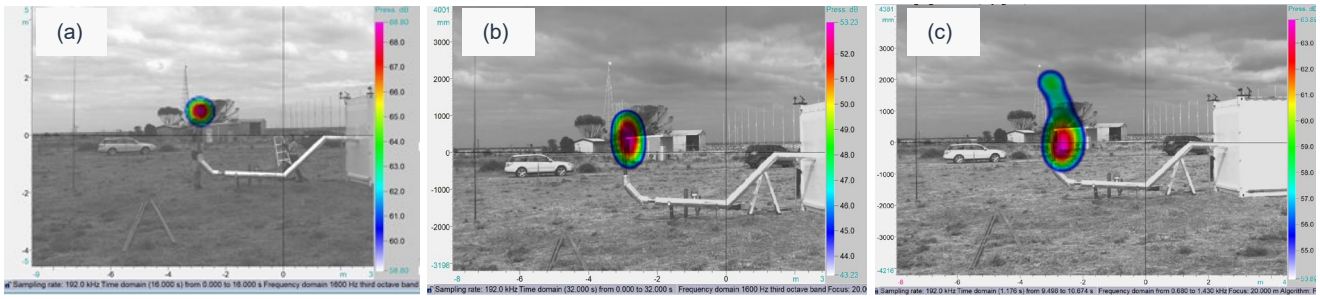

Figure 14 – Acoustic field observed by the 48 microphone gfai tech ring array. (a) 50mm compression driver: SPL 1.6 kHz one-third octave band, (b) hot exhaust stack with the turbine operating at 43,800 RPM: SPL 1.6 kHz one-third octave; and (c) “bubbles” of sound observed from turbine exhaust when wind gusts are present: SPL 1 kHz octave band.

Results – Acoustic cameras: Figure 14 shows the sound fields viewed by the cameras placed downwind of the outlet from three test cases: (a) a 50 mm compression driver acting as a monopole source, (b) the hot exhaust for low (1–3 m/s) crossflow velocities, and (c) the same operating condition for the turbine but with stronger (4–8 m/s), gusty crossflow. All figures are for low frequencies, well below cut-on of higher order modes ($ka < 1$). Figure 14(a) and (b) are for the 1600 Hz one-third octave band, which for the compression driver has a non-dimensional Helmholtz frequency of $ka = 0.7$, and the exhaust is $ka = 0.95$. Figure 14(c) shows the SPL in the 1 kHz octave band, which gives a Helmholtz number of $ka = 0.6$. The octave band was used instead of the one-third octave band due to gusty conditions affecting image stability. Given the low frequencies, in the absence of temperature or velocity gradients, all radiation patterns should be approximately spherical. Figure 14(a) shows a circular radiation pattern consistent with a monopole source and spherical radiation. However, Figure 14(b) and (c) exhibit very different radiation patterns, with the source being extended in the vertical direction and more closely resembling a finite line source. This is consistent with a sound being refracted downwards by the exhaust stream. It was observed that the stronger the crosswind the larger the extent of the source in the vertical direction, and under gusty conditions the source could extend up to 10 diameters in the vertical.

Results – Microphone Arrays: The fixed microphone arrays were used to quantify the sound field at the exhaust plane. The exhaust-plane directivity (collected for 120 s) from the circumferential microphone arrays is presented in Figure 15(a) and (b), with geometric spreading observed from the corresponding longitudinal array in Figure 15(c). Figure 15 (a) shows that the peak in the far-field SPL occurs downstream (indicated by red dashed line), with the downstream SPL 9 dB higher (and up to 11 dB higher when measured over shorter time frames) than upstream SPLs. Figure 15 (b) was used to characterise the stability of the far-field SPL by plotting the difference between L_{10} and L_{90}, where it can be seen that the downwind SPL is far less stable than upwind by at least 6 dB, and was often observed to be >9 dB higher. Figure 15(c) plots the SPL versus distance from the outlet, where the SPL for the compression driver (upwind and downwind) and the SPL upwind of the turbine outlet exhibit –6 dB per doubling of distance. However, the downwind SPL falls less steeply at approximately –4.8 dB per doubling in distance, and at a distance of $256D$, the SPL is 3 dB higher than upwind and 6 dB higher than predicted. The slight uptick in both driver and upstream SPLs at $256D$ are associated with background noise. It is worth noting that the geometric expansion rate of ~ –4.8dB per doubling in distance was also observed in the numerical models presented in Section 3.4, and not too dissimilar to Equation (3) that gives –4.0 dB per doubling in distance.

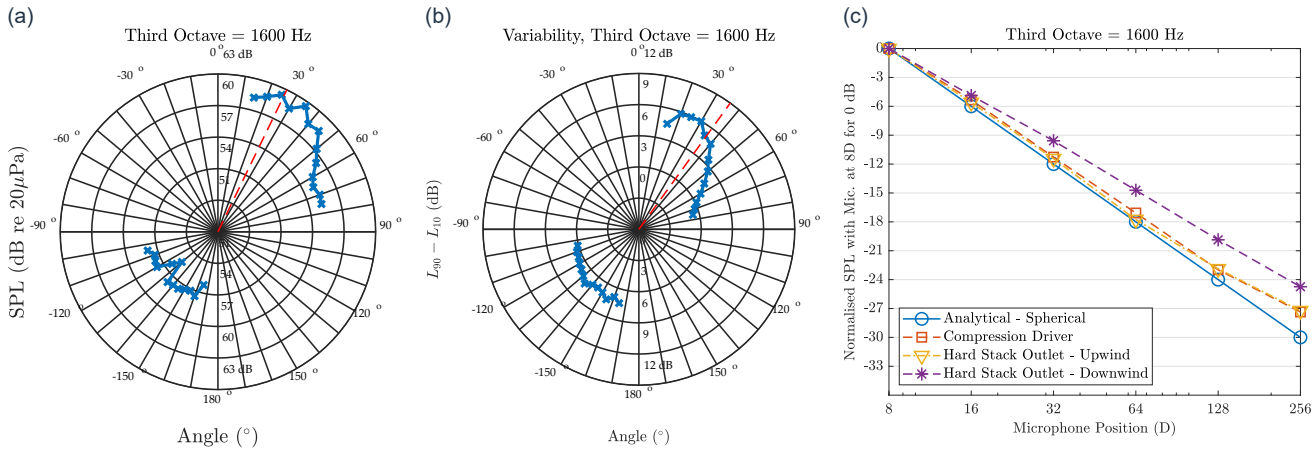

Figure 15 – Ground-plane directivity at 1600 Hz ($ka = 0.95$). (a) circumferential array SPL at $200D$ from outlet; (b) SPL stability $L_{10} - L_{90}$ at $200D$; and (c) longitudinal array geometric spreading $8D - 256D$.

3.4 Coupled CFD-FEA computational aero-acoustics modelling on a supercomputer

The sound refraction through the exhaust plume has been simulated using a coupled CFD-FEA computational aero-acoustics model for both a ground jet in crossflow and an elevated jet in crossflow. The details of the ground level jet in crossflow can be found in (Leav O. , Cazzolato, Howard, & Mabrouk, 2023). The numerical approach used a RANS CFD model solved in ANSYS FLUENT to determine the temperature and velocity field for the jet in crossflow. These two fields were then imported into ANSYS Mechanical to solve a finite element scalar potential formulation of the acoustic field, with an upper bound on the frequency of $ka \leq 0.8$ and crossflow ratio of $R \leq 7.5$. The methodology and the model domain are shown in Figure 16.

Ground jet in crossflow: Early numerical modelling of the sound refraction through the exhaust plume from a ground level jet in cross-flow was done to reduce the complexity of the model and analyse the effects of the plume on sound radiation. Figure 17 plots sound directivity for $ka = 0.8$ as an isometric view and a cross section in the vertical plane in the direction of the crosswind for a Mach number $M_j = 0.1$ and jet temperature $T_j = 500°\text{C}$. The results from the numerical simulations highlighted the effects of the flow and temperature from the exhaust plume on the sound refraction, with increases in downwind directivity index (DI) of up to 10 dB along the ground plane at $32D$. The authors recommend referring to (Leav O. , 2020) and (Leav O. , Cazzolato, Howard, & Mabrouk, 2023) for more detailed discussions regarding the numerical simulation results for sound propagation through ground level jet in crossflow, where parameters effecting sound directivity such as temperature, frequency, and jet to crossflow momentum ratio (R) are elaborated upon.

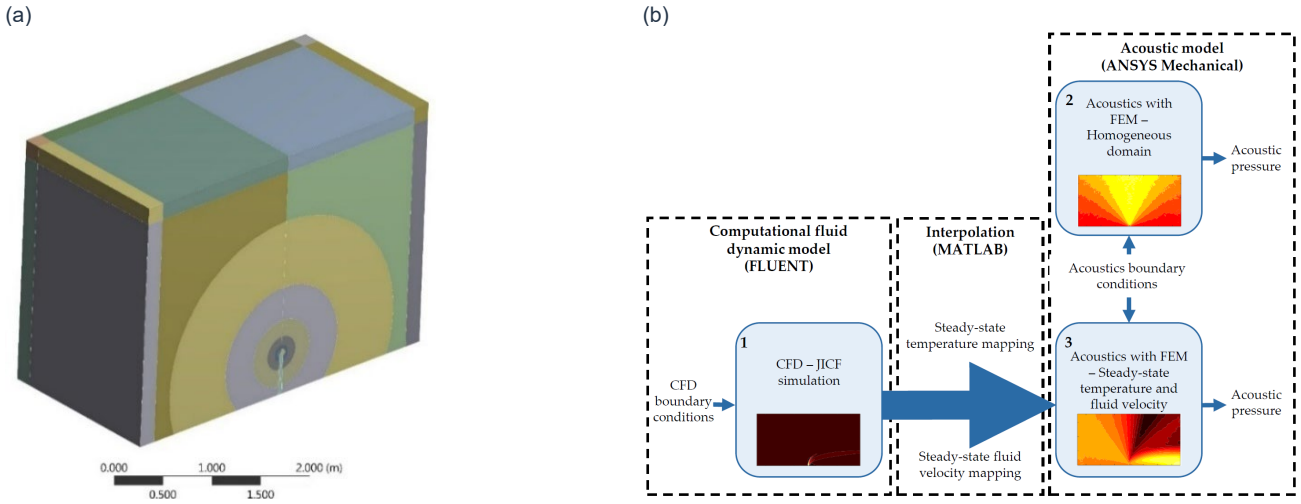

Figure 16 – (a) CFD and FEA domain, (b) method used to solve the coupled computational aero-acoustic model.

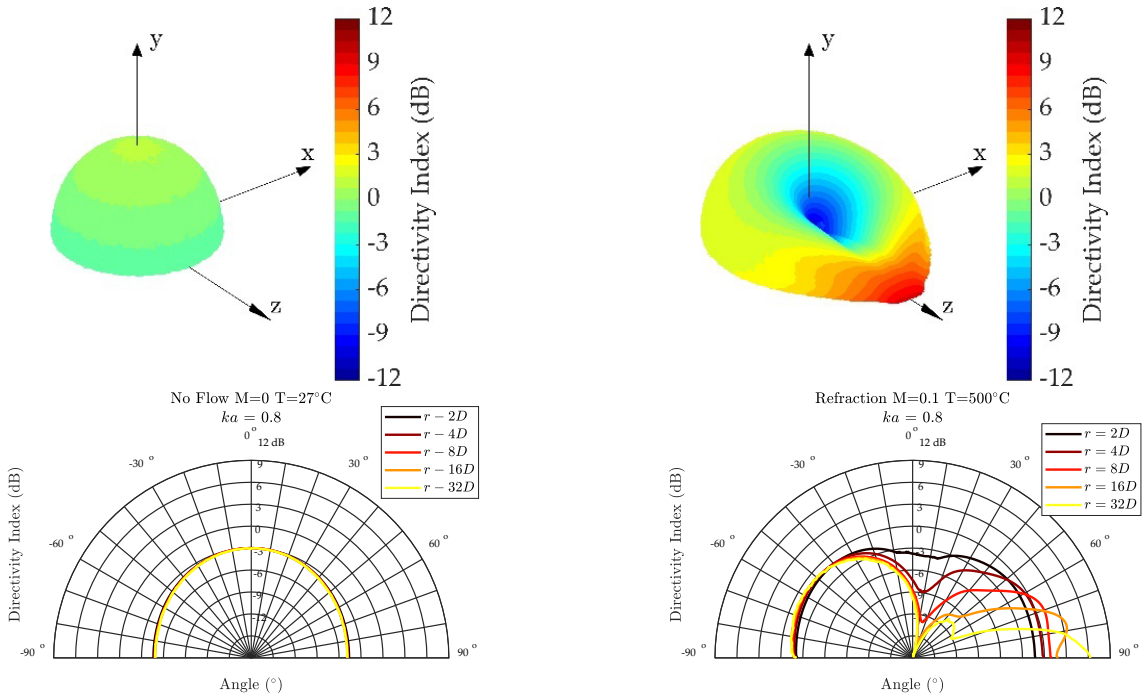

Figure 17: Sound directivity of $ka = 0.8$ as an isometric view (upper row) and corresponding cross section in the vertical plane in the direction of the crosswind (lower row); (left column) no jet, and (right column) jet in crossflow for a Mach number $M_j = 0.1$ and jet temperature $T_j = 500°C$.

Elevated jet in crossflow: Recently we have also modelled an elevated jet in crossflow. The findings are similar to the results of the ground jet in crossflow presented previously. Figure 18 plots sound directivity for the 3150 Hz one-third octave band ($ka = 0.85$) as an isometric view and a cross section in the vertical plane in the direction of the crosswind for a Mach number $M_j = 0.1$ and jet temperature $T_j = 500°C$. The ripples in the sound field are associated with low element density (relative to wavelength) and insufficient absorption at the boundaries of the domain. What is immediately apparent is the rapid convergence of results versus distance for the homogenous media and the vertical jet. However, the elevated jet with crossflow has not converged at $32D$ downwind, with the lobe 9 dB stronger than the monopole (0 dB) and 12 dB stronger than the open pipe at the horizontal (–3 dB).

Figure 19 illustrates the strong frequency dependence of the directivity when there is crossflow, comparing two adjacent one-third octave bands, namely 2500 Hz ($ka = 0.67$) and 3150 Hz ($ka = 0.85$). For frequencies lower than shown here, the strength of the lobe weakens, and for higher frequencies it increases.

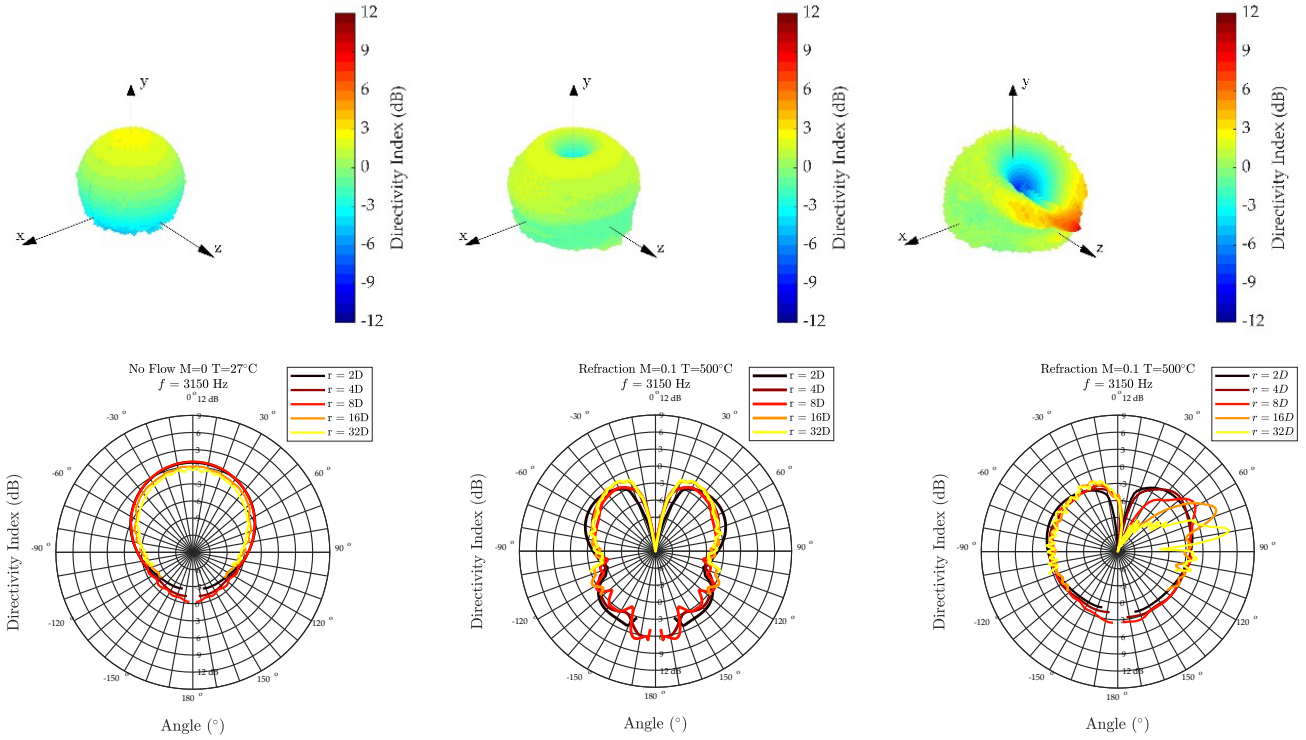

Figure 18 – Sound directivity of the 3150 Hz one-third octave band ($ka = 0.85$) as an isometric view (upper row) and corresponding cross section in the vertical plane in the direction of the crosswind (lower row) for a Mach number $M_j = 0.1$ and jet temperature $T_j = 500°C$. From left to right is open pipe in homogenous media, elevated vertical jet, and elevated jet in crossflow.

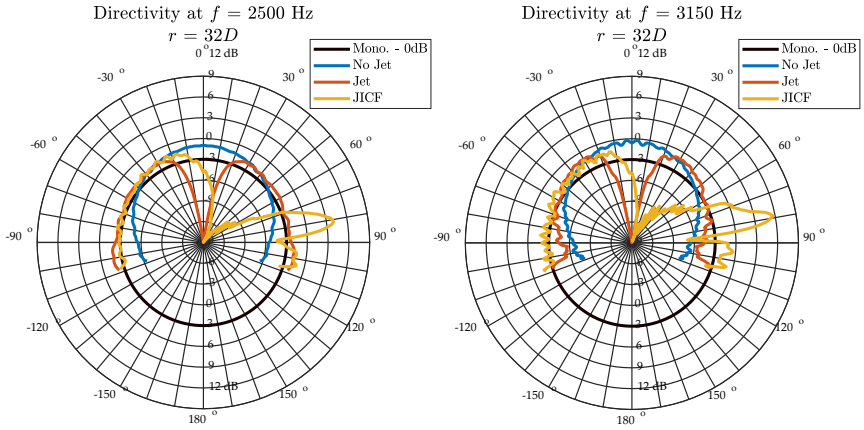

Figure 19 – Sound directivity for a monopole, open pipe in homogenous media (no jet), vertical jet and jet in crossflow at $32D$ for a Mach number $M_j = 0.1$ and jet temperature $T_j = 500°C$. Left image the 2500Hz one-third octave band ($ka = 0.67$), right image the 3150Hz one-third octave band ($ka = 0.85$).

4 CONTROLLING SOUND REFRACTION THROUGH JETS IN CROSSFLOW

As a way of validating the hypothesis that the exhaust plume was responsible for the large increase in downwind SPLs, a second campaign was undertaken. An acoustically transparent nozzle, which permitted the flow of acoustic energy but not the bulk gas flow, was conceived (Japanese Patent No. 7525906, 2024) and tested in the wind tunnel, field and using numerical simulations. This concept is illustrated in Figure 20; as the length of the nozzle increases the situation approaches the no crossflow case (that is, the plume remains columnated and downwind refraction should be reduced). The outcomes from the investigation are presented in the following sections and is based on (Leav O. , 2020), (Leav, Cazzolato, & Howard, 2023) and (Cazzolato, Leav, & Howard, 2023).

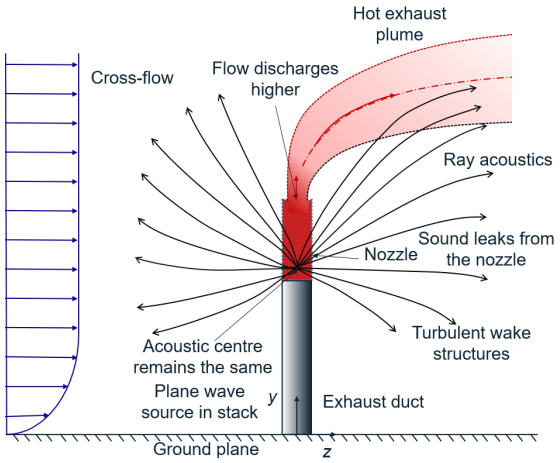

Figure 20 – Schematic illustrating the concept of an acoustically permeable, flow impermeable nozzle.

4.1 Wind tunnel experiments 1:125 scale

Three different exhaust nozzles (a straight section, a conical section and a venturi) were tested in The University of Adelaide Wind Tunnel and are shown in Figure 21. The nozzles were constructed from two different layers of stainless-steel mesh: a fine 300 grade stainless steel mesh (0.05mm open hole sizing and 0.05mm thickness) for high flow resistivity (impervious to flow), and a coarse 50 grade (0.282mm open hole sizing and 0.2mm thickness) stainless steel mesh form the shape of the nozzle. All three nozzles were $6D$ (~300 mm) in length. The insertion loss of each nozzle was measured and found to be negligible in the frequency range of interest. A plot comparing the directivity (at a distance of $28D$ from the outlet) of the various end conditions is shown in Figure 21(c) for a frequency of 3150 Hz ($ka = 0.85$). Upwind, the nozzles had no significant impact on the SPL directivity, as would be expected from the results presented in Section 3. However, the transparent nozzles were found to reduce the peak downwind SPLs by 3–5 dB, depending on frequency.

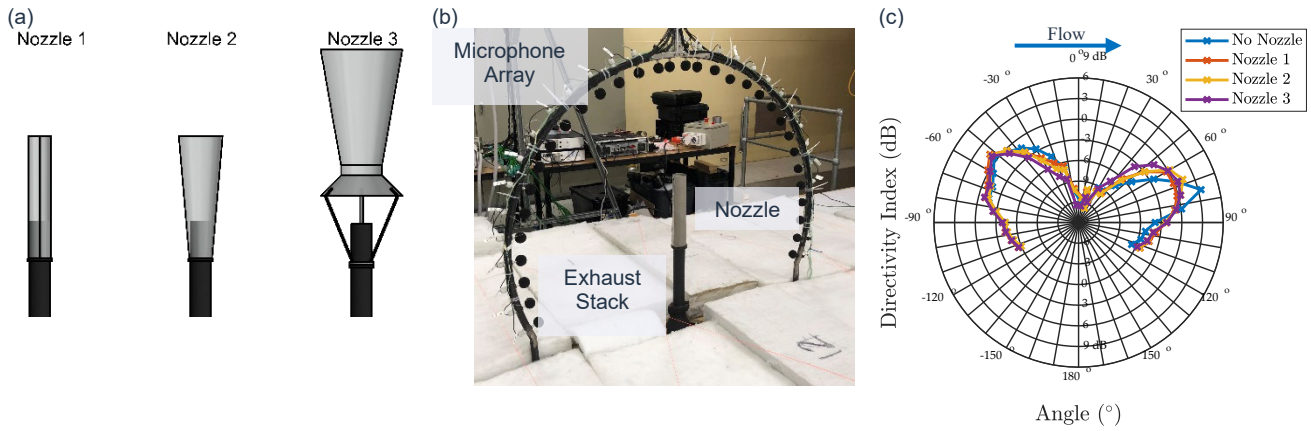

Figure 21 – (a) Three transparent nozzles: Nozzle 1 - straight cylindrical section, Nozzle 2 - conical section with 5° expansion, and Nozzle 3 -venturi section nozzle, (b) image of Nozzle 1 being tested in the wind tunnel, (c) sound directivity in the exhaust plane.

4.2 Coupled CFD-FEA computational aero-acoustics modelling on a supercomputer

The acoustically transparent stack was also modelled numerically, with the results shown in Figure 22. The results are similar to the wind tunnel experiments, with the SPL of the downwind lobe reducing by 4–5 dB (at a distance of $32D$ from the exhaust). It should be noted that the radiated acoustic energy remained unaffected in this process and convergence of the refraction process had not been achieved at the limits of the domain ($32D$).

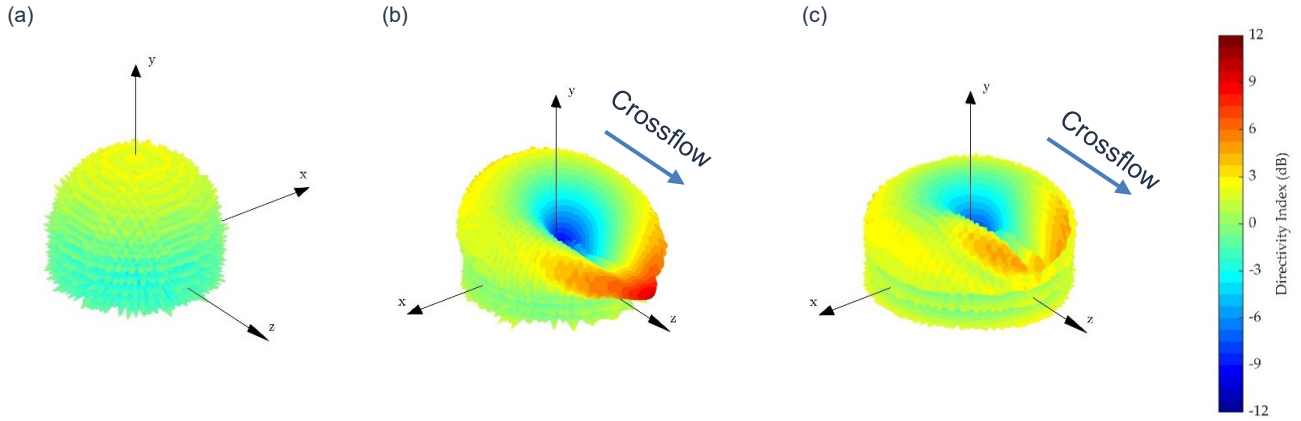

Figure 22 – Numerical simulations of sound directivity at $ka = 0.85$ (a) no jet, (b) hot jet in crossflow and hard stack, (c) hot jet in crossflow with transparent stack.

4.3 Field experiments on a 1:60 scale turbojet engine

Five acoustically transparent stack geometries were tested on the SR-30 turbojet engine (Figure 23(a)): (1) $6D$ (in length) transparent, (2) $4D$ transparent, (3) $4D$ 50 mm thick muffler, (4) $4D$ 25 mm thick muffler, and (5) $2D$ 25 mm thick muffler. All nozzles used a 51% open area perforated steel and woven steel cloth. The muffler designs had Durablanket ceramic fibre liners with mean airflow resistivity of 81,500 Pa.s/m^2. The acoustic insertion loss (IL) of the nozzles were measured in a reverberation chamber (Figure 23 (b) and (c)), with the transparent nozzles exhibiting negligible insertion loss, and the mufflers providing between 6 dB and 18 dB reduction within the frequency range of interest (500–10 kHz), with the thicker and longer muffler providing the most attenuation.

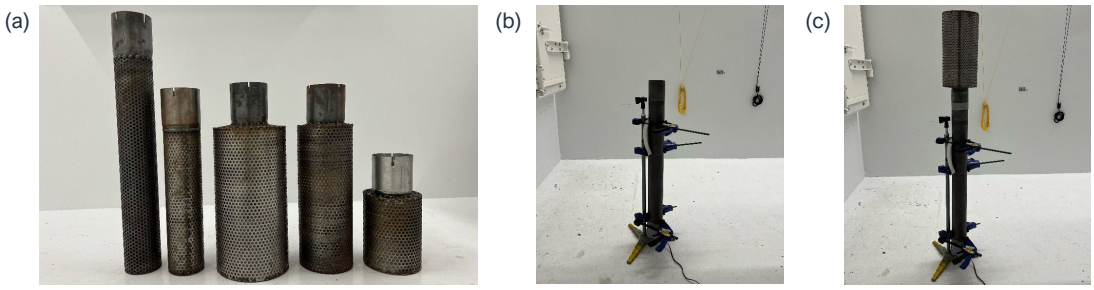

Figure 23 – (a) Five acoustically transparent nozzles, (b) testing IL of hard stack, (c) testing IL of transparent stack.

Figure 24 compares the SPLs from the hard outlet and the $6D$ acoustically transparent nozzle $64D$ downwind of the outlet at ± 1 m $\approx \pm 10°$ above and below the exhaust plane. The SPLs above the outlet are considerably higher than below, which is consistent with the directivity patterns with crossflow seen in the previous sections. It is also immediately clear that despite the transparent nozzle providing zero insertion loss, the downwind SPLs with the transparent nozzle are reduced by up 10 dB in the frequency range of interest ($0.5 \leq ka \leq 2$).

Figure 25 compares the most effective two nozzles: the 25 mm thick $4D$ muffler, which provided both attenuation as well as mitigation of refraction, followed closely by the $6D$ acoustically transparent nozzle. Interestingly, at the main lobe (measured by the upper microphone) the $6D$ acoustically transparent nozzle outperformed 25 mm thick $4D$ muffler at low frequencies ($0.5 \leq ka \leq 1$), whereas the muffler was fractionally better above $ka \geq 1$.

5 DISCUSSION

The work presented here, where possible, has maintained dimensional consistency with full scale OCGTs as shown in Table 1. It is important to note that downwind directivity is strongly dependent on the trajectory of the plume, and that atmospheric and temperature gradients have a strong influence on buoyant plumes. Hence SPLs from OCGTs are expected to vary from the models presented here. However, it is also worth noting that the SPL magnitudes observed in the models are consistent with observations in the field with real OCGTs.

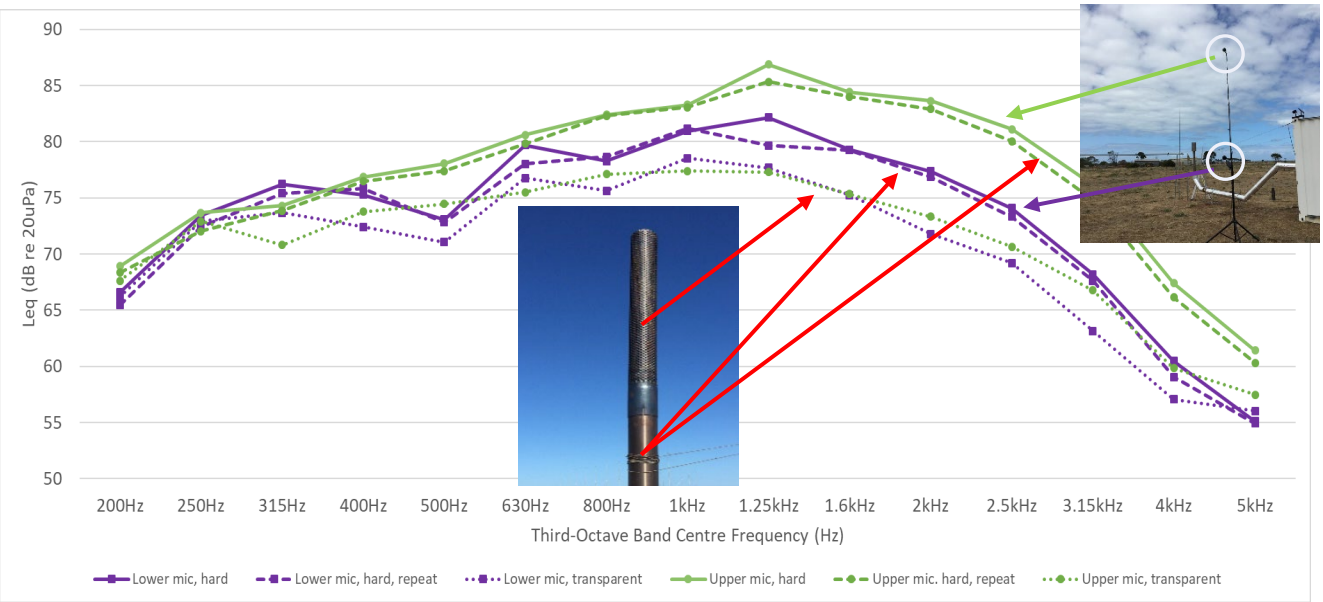

Figure 24 – Comparison of sound pressure levels at $64D$ downwind of the outlet for a hard stack and the $6D$ acoustically transparent nozzle. Measurements were $\pm 1m \approx \pm 10°$ above (green) and below (purple) the exhaust plane.

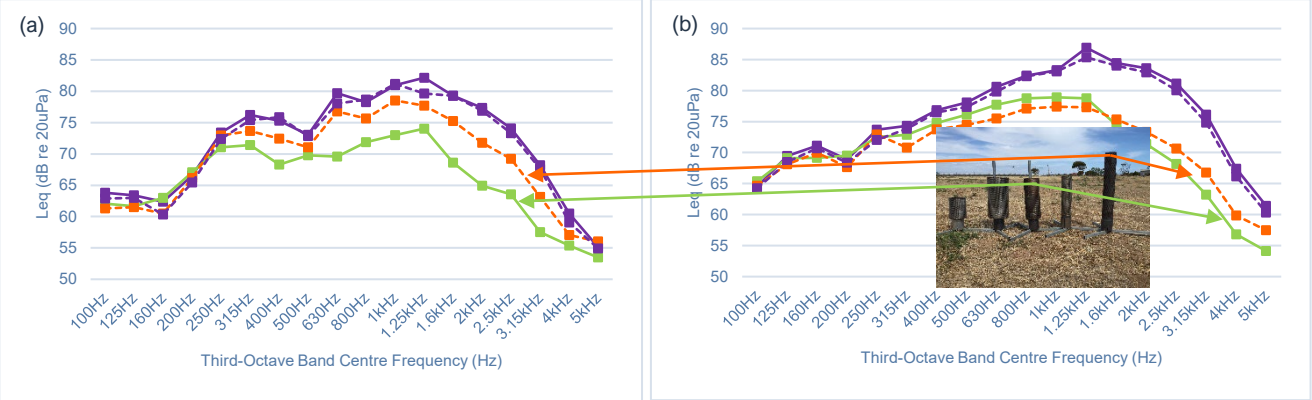

Figure 25 – Comparison of SPLs at $64D$ downwind of the outlet for a hard stack (purple), the $6D$ transparent nozzle (orange), and 25mm thick $4D$ muffler (green). (a) 1m below the exhaust plane, (b) 1m above the exhaust plane.

6 CONCLUSIONS

The work presented above has conclusively shown that the sound from hot exhausts is affected by refraction. In the absence of crossflow, ground-plane SPLs can be 1–2 dB higher than a monopole, and 2–5 dB higher than an open pipe without flow in the far-field. With crossflow, SPL increases of between 8–12 dB have been observed in simulations, wind tunnel experiments, small-scale field trials and from full-scale OCGTs. Acoustically transparent stacks have been shown to partially mitigate this increase with simulations (reductions of 6–9 dB at $32D$), wind tunnel experiments (reductions of 3–8 dB at $28D$) and field experiments (reductions of 8–11 dB at $64D$). It is recommended that when predicting community noise levels from OCGTs the directivity patterns presented in this paper are used in sound propagation models for downwind receivers, or alternatively, a geometric spreading rate of –4.8 dB (as opposed to –6 dB) per doubling in distance be applied to the low frequency components ($0.5 \leq ka \leq 2$). If a simple rule of thumb is required, then adding 10 dB to predicted levels is reasonable.

ACKNOWLEDGEMENTS

The authors would like to acknowledge Chris Turnbull, Linjun Zhao, Lauren Manser, Carl Jungfer, Ben Wake, Brent Poland and Haris Amin in the collection of this data and generation of ideas. HT Technologies and Resonate Acoustics for the use of their acoustic cameras, and finally, the financial support of the AAS Research Grant.

Table 1 – Comparison of non-dimensional parameters for real OCGTs and modelling at the University of Adelaide.

	Variable	Real OCGT	Anechoic Chamber	Wind Tunnel Experiments	Buckland Park Experiments	CFD/FEA
Scale	-	1:1	1:200	1:125	1:60	1:125
Duct Diameter (m)	D	6.00	0.027	0.0476	0.0984	0.0476
Mach Number	M	0.09	0.10	0.10	0.06-0.12	0.10
Maximum Temperature (K)	T_{max}	703-953	431	773	643-873	773
Temperature Ratio	Θ	3.18	1.59	2.58	2.91	2.58
Crossflow Momentum Flux Ratio	R	3-20	∞	5-12.5	2.5-20	5.00
Helmholtz Number	ka	0.53-3.19	0.8-1.2	0.85-1.70	0-5.5	0.3-1.05
Max Distance from Source	L/D	500	27	28	256	32
Reynolds Number	Re	3,170,000	18,000	32,761	40,776-71,192	32,761

REFERENCES

Atvars, J., Schubert, L., & Ribner, H. (1965). Refraction of sound from a point source placed in an air jet. *JASA, 37*, 168–170.

Atvars, J., Schubert, L., Grande, E., & Ribner, H. (1966). *Refraction of sound by jet flow or jet temperature.* Institute for Aerospace Studies. University of Toronto.

Bradbury, L. (1981). Some aspects of jet dynamics and their implications for VTOL research. *NATO AGARD*, (pp. 1.1-2).

Cazzolato, B., Hansen, C., Robertson, W., & Zhao, I. (2013). Sound directivity from high temperature exhaust stacks. *Australian Acoustical Society AAS2013 Victor Harbor - Science, Technology and Amenity.*

Cazzolato, B., Leav, O., & Howard, C. (2021). Sound directivity from a 250kW gas turbine exhaust system. *Proceedings of Acoustics 2021* (p. 8). Wollongong: Australian Acoustical Society.

Cazzolato, B., Leav, O., & Howard, C. (2023). Environmental noise from open-cycle gas turbines. *ICSV29.* Prague: IIAV.

Cazzolato, B., Leav, O., & Howard, C. (2023). When less is more: Reducing environmental noise from open cycle gas turbines with acoustically transparent stacks. *JASA, 154*(4 Supplement). doi:10.1121/10.0022936

Cazzolato, B., Leav, O., Howard, C., & Turnbull, C. (2024). *Japanese Patent No. 7525906.*

Hessler, G. J. (2004). Proposed criteria in residential communities for low-frequency noise emissions from industrial sources. *Noise Control Engineering Journal, 52*, 179–185. doi:10.1260/0263092054530957

Hetzel, R., & Robert, P. A. (2009). Sources and rating criteria of low frequency gas turbine exhaust noise - via case study. *Inter-noise 2009*, (pp. 1-8). Ottawa.

ISO 9613-2. (2024). *Acoustics — Attenuation of sound during propagation outdoors. Part 2: Engineering method for the prediction of sound pressure levels outdoors.*

Leav, O. (2020). *An investigation into the mechanics of sound propagation through turbulent non-isothermal exhaust jets in cross-flow.* University of Adelaide.

Leav, O., Cazzolato, B. S., & Howard, C. (2023). Lab-scale research on acoustically transparent stacks for hot exhaust jets in cooler cross-flow. *JASA, 154*, 1-10. doi:10.1121/10.0023559

Leav, O., Cazzolato, B., & Howard, C. (2021). Sound propagation through elevated, heated jets in cooler cross-flow: An experimental study. *JASA, 150*(1), 82-93. doi:10.1121/10.0005489

Leav, O., Cazzolato, B., Howard, C., & Mabrouk, B. (2023). Steady-state sound propagation through hot exhaust jets in cooler cross-flow: A computational study. *JASA, 154*, 217-231. doi:10.1121/10.0020069

Manning, C. J. (1981). *The Propagation of Noise From Petroleum and Petrochemical Complexes To Neighbouring Communities. Technology.*

Mungur, P., Plumblee, H., & Doak, P. (1974). Analysis of acoustic radiation in a jet flow environment. *JSV, 36*(1), 21–52.